Photoinduced reactivity in a dispiro-1,2,4-trioxolane: adamantane ring expansion and first direct observation of the long-lived triplet diradical intermediates

Elisa M. Brás,[a,c] Lília I. L. Cabral,[a,b] Patrícia S. M. Amado,[a,b] Manabu Abe,[d] Rui Fausto[c,*] and Maria L. S. Cristiano[a,b,*]

[a] *Centro de Ciências do Mar (CCMAR), Universidade do Algarve, Campus Gambelas, Faro, Portugal.*
[b] *Departamento de Química e Farmácia, Faculdade de Ciências e Tecnologia, Universidade do Algarve, Campus de Gambelas, Faro, Portugal.* [c] *CQC, Department of Chemistry, University of Coimbra, Portugal.*
[d] *Department of Chemistry, Graduate School of Science, Hiroshima University, Hiroshima, Japan.*

ABSTRACT

The dispiro-1,2,4-trioxolane **1**, an ozonide with efficient and broad antiparasitic activity, was synthesized and investigated using matrix isolation FTIR and EPR spectroscopies together with both B3LYP/6-311++G(3df,3dp) and M06-2X/6-311++G(3df,3dp) theoretical methods. Irradiations ($\lambda \geq 290$ nm) of the matrix isolated **1** (Ar or N_2) afforded exclusively 4-oxahomoadamantan-5-one **4** and 1,4-cyclohexanedione **5**. These results suggested that the reaction proceeded *via* a dioxygen-centered diradical intermediate, formed upon homolytic cleavage of the labile peroxide bond, which regioselectively isomerized to form the more stable (secondary carbon-centered)/oxygen-centered diradical. *In situ* EPR measurements during the photolysis of **1** deposited in a MeTHF-matrix led to the detection of signals corresponding to two triplet species, one of which was short-lived while the other proved to be persistent at 10 K. These observations strongly support the proposed mechanism for the photogeneration of **4** and **5**, which involves intramolecular rearrangement of the intermediate diradical species **2** to afford the triplet diradical **3**.

* Corresponding authors e-mails:
R.F.: rfausto@ci.uc.pt
M.L.S.C.: mcristi@ualg.pt

INTRODUCTION

Organic dispiro-endoperoxides, in particular dispiro 1,2,4-trioxanes and 1,2,4-trioxolanes (ozonides), have been attracting much attention since the discovery of artemisinin more than 40 years ago[1-3], which provided a completely new antimalarial structural prototype of pharmacophore. The mechanism of bioactivation and action of the artemisinins and related endoperoxide based drugs has been discussed thoroughly[4-14] and bioactivation is known to require iron(II)-induced reductive cleavage of the peroxide bond to form oxygen-centered radicals, followed by rearrangement to generate carbon-centered radical species that act through modification of parasites biological targets. From a synthetic point of view, endoperoxides are useful for preparation of different types of compounds *via* ring expansion reactions[15], and also for the synthesis of α-keto acids[16] *cis*-diols[17], 1,2-diol monoesters[18,19], benzofurans and benzopyrans[20] *via* selective ring cleavage.

In all the above chemical processes, radical or diradical species have been hypothesized to be the key reactive intermediates, following the initial homolytic cleavage step. For asymmetrically substituted dispiro-1,2,4-trioxolanes, represented by compound **1**, and also for their dispiro-1,2,4-trioxane analogues, it has been postulated, based on the final reaction products obtained, that after the cleavage of the peroxide bond generating the dioxygen-centered diradical **2** a regioselective β-scission occurs concomitantly with the rearrangement, leading to the carbon-centered/oxygen-centered diradical species **3** (see Scheme 1)[21-23].

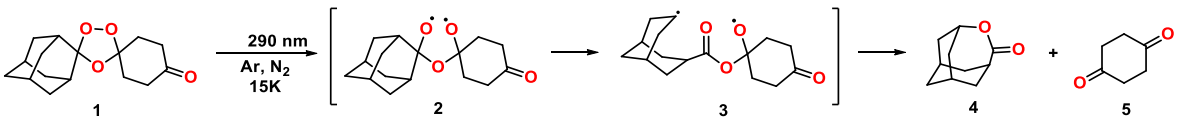

Scheme 1. Generic mechanistic scheme for a representative reaction of a dispiro-1,2,4-trioxolane starting with the homolytic cleavage of the O–O bond. The example chosen relates with the present study, where the reaction took place in a cryogenic matrix (either solid Ar or N_2, at 15 K), the substituents of the trioxolane core being the spiroadamantyl and spiro-*p*-cyclohexanonyl groups and using UV light ($\lambda \geq 290$ nm) as the reaction initiator.

When Fe(II) is involved in the reaction, as during the Fe(II)-induced cleavage of the antimalarial peroxides, the metal ion binds to the radical species[4-14]. In spite of the

accumulated evidence of the participation of radicals or diradicals in all these types of reactions, and also of the successful detection of some of these species for reactions involving cyclic peroxides[24, 25], the experimental detection and characterization of the diradical species following the homolytic peroxide bond cleavage of dispiro-1,2,4-trioxolanes has not been reported hitherto.

In the present article, we report the first direct observation of the two claimed diradical intermediates for this type of reaction. The strategy used to achieve this goal started with the identification of the final products of the UV-induced unimolecular photolysis of adamantane-2-spiro-3'-8'-oxo-1',2',4'-trioxaspiro[4,5]decane (**1**) isolated in low temperature matrices (argon and N_2), and their vibrational characterization. Subsequently, the EPR spectroscopy was used to search for the involved diradicals generated under UV-photolysis of the compound isolated in a low temperature MeTHF matrix. The choice for the low temperature solid state media to perform this investigation was motivated by three main reasons: (1) under these conditions, because the molecules of the precursor are cage-confined and diffusion does not take place[26-30], no products can be expected to be formed resulting from species produced from fragmentation of different molecules; this considerably simplifies the accessible chemistry, thus allowing to focus on the main features of the mechanism of the reaction; (2) due to the low work temperature (of a few K) the attainable spectral resolution is much higher compared to what can be obtained, for example, in solution[26-30]; together with absence of significant interactions with the host material this feature allowed to obtain data of better quality for structural elucidation and, at the same time, that could be directly compared with results of quantum chemical computational predictions, which were done for the isolated molecules *in vacuo*; (3) finally, it could also be expected that the lifetime of the intermediates were longer under the used experimental conditions (low temperature; inhibited molecular diffusion; relative inertness of the medium), so that their experimental detection would be facilitated.

As described in detail below, the obtained results demonstrate that the UV-induced photolysis of the investigated dispiro-1,2,4-trioxolane proceeds regioselectively, leading to its adamantane substituent ring expansion, *via* the two key diradical triplet species suggested previously, which could be successfully detected here for the first time by EPR spectroscopy. As it could be expected, the measured lifetimes of the two diradicals differ considerably, with

the carbon-centered/oxygen-centered diradical being considerably more stable than its oxygen centered diradical precursor.

It is worth noting that trioxolane **1** has very relevant and broad antiparasitic properties. It has shown low nanomolar activity against *Plasmodium falciparum*[31] and recent studies demonstrated that its activity is retained against *P. falciparum* strains resistant to chloroquine and to the artemisinin-derived drugs used in combination therapies (ACT)[32]. Compound 1 also exhibits low micromolar activity against intracellular amastigote forms of *Leishmania infantum*[33] and against *Perkinsus olseni*[34]. In addition to its broad antiparasitic activity, the studied compound can be prepared from the commercially available 2-adamantanone and 1,4-cyclohexanedione building blocks in only 2 steps.

EXPERIMENTAL AND COMPUTATIONAL DETAILS

General

Commercial reagents were used as purchased. ^{1}H and ^{13}C-NMR spectra were recorded on a 400 MHz NMR spectrometer Bruker Avance III 400. ^{1}H-NMR-chemical shifts are referred to the residual signal of $CDCl_3$ (δH 7.26) and ^{13}C-NMR-chemical shifts to the $CDCl_3$ signal (δC 77.0), or using TMS as internal standard. Thin-layer chromatography was carried out on silica gel 60 F254 plates (AL TLC 20x20). Column chromatography was performed on Silica Gel 60 (0.04 – 0.063 mm). Melting points (°C) were obtained on a SMP3 Melting Point Apparatus and are uncorrected.

Syntheses and general characterization of the compounds

Adamantane-2-spiro-3'-8'-oxo-1',2',4'-trioxaspiro[4,5]decane 1: ozone, produced with an ozone generator Sander Labor-Ozonizator 301.7 (0.5 L/min O_2, 140 V), was passed through a solution of dichloromethane at –78 ºC and flushed into a solution of *O*-methyl 2-adamantanone oxime (1.00 g, 5.58 mmol) and 1,4-cyclohexanedione (0.65 g, 5.58 mmol) in pentane (60 mL) and dichloromethane (40 mL) at 0 ºC. After consumption of the starting material, the solution was flushed with nitrogen for 5 min and concentrated under reduced pressure at room temperature to give a crude material. Purification by flash chromatography using a mixture of EtOAc/*n*-hexane, gave the pure compound as a colorless solid (0.66 g, 42% yield): m.p. 127-128 ºC; ^{1}H-NMR (400 MHz, $CDCl_3$): δ 1.69-2.02 (m, 14H), 2.14 (t, *J*

= 6.9 Hz, 4H), 2.51 (t, J = 7.0 Hz, 4H) ppm; ^{13}C-NMR (100 MHz, $CDCl_3$): 25.9, 26.31, 31.09, 32.59, 34.25, 35.70, 36.18, 37.35, 106.46, 111.95, 208.90 ppm; MS (EI, *m/z*): 278.9 $[M]^+$.

The *O*-methyl 2-adamantanone oxime precursor of compound **1** was obtained as follows: to a solution of 2-adamantanone (4.00 g, 26.63 mmol) in methanol (20 mL), under stirring, was added pyridine (3.40 mL, 42.03 mmol) and methoxylamine hydrochloride (2.846 g, 34.08 mmol). The reaction mixture was stirred at room temperature for 72 h. The final mixture was concentrated and then diluted with dichloromethane (20 mL) and water (30 mL). The organic layer was separated, and the aqueous layer was washed with dichloromethane (2x20 mL). The combined organic layers were washed with aqueous HCl (1 M; 20 mL x2), then with brine (20 mL). The final organic extract was dried with $MgSO_4$, filtered, then concentrated under reduced pressure to give *O*-methyl-2-adamantanone oxime (4.20 g, 88% yield) as a colorless solid (m.p. 69-70 ºC). ^{1}H-NMR (400 MHz, $CDCl_3$): δ 3.81 (s, 3H), 3.46 (s,1H), 2.54 (s, 1H), 2.00 – 1.78 (m, 12H) ppm. ^{13}C NMR (101 MHz, $CDCl_3$) δ: 166.74, 60.96, 39.03, 37.64, 36.52, 36.24, 29.53, 27.85 ppm. MS (MALDI-TOF, *m/z*): 180.02 $[M]^+$.

4-Oxahomoadamantan-5-one 4, was synthesized using the procedure described by Renoud-Grappin *et al*.[35] To a suspension of 2-adamantanone (0.5 g, 3.33 mmol) and $NaHCO_3$ (0.31 g, 3.66 mmol) in anhydrous dichloromethane (10 mL) was added a solution of *m*-chloroperoxybenzoic acid (*m*-CPBA) (0.86 g, 4.99 mmol) in anhydrous dichloromethane (5 mL). The reaction mixture was stirred at room temperature, in the dark, until consumption of the starting compound. Then the organic mixture was washed with water (3x15 mL), brine (2x15 mL) and dried over with $MgSO_4$. The organic layer was then evaporated to dryness under reduced pressure. Purification of the residue by flash chromatography using a mixture of EtOAc/*n*-hexane, gave the required product as a white solid (0.35 g, 63% yield): m.p: 288-290 ºC. ^{1}H NMR (400 MHz, $CDCl_3$): δ = 4.49 (tt, J = 4.4, 2.4 Hz, 1H), 3.10 – 3.05 (m, 1H), 2.16 – 1.58 (m, 12H). ^{13}C NMR (101 MHz, $CDCl_3$): δ = 178.99, 73.17, 41.24, 35.78, 33.82, 30.96, 25.85. HRMS (CI, *m/z*) calcd for $C_{10}H_{15}O_2$ $(M+H)^+$: 167.1067; found 167.1072.

1,4-Cyclohexanedione 5 was purchased from Sigma Aldrich UK and used without further purification.

All compounds prepared were kept in the freezer and shielded from the light during storage, remaining stable under these conditions.

Matrix isolation infrared spectroscopy measurements

To prepare the low temperature matrices a sample of the solid compound to be studied was placed in an especially designed thermoelectrically heatable mini-oven attached to the vacuum chamber of a helium cryostat (APD Cryogenics closed-cycle helium refrigerator system with a DE-202A expander). Before the measurements, the samples were subjected to additional purification by continued high-vacuum ($\sim 10^{-7}$ mbar) pumping, during approximately 1 hour, at room temperature. The samples were then sublimed and the vapors of the compound to be studied were deposited, together with a large excess of argon or N_2, onto a cesium iodide (CsI) substrate mounted at the cryostat cold tip (15 ± 0.1 K, as measured by a silicon diode sensor connected to a Scientific Instruments digital temperature controller). This temperature was kept during the overall experiments.

The IR spectra of the matrix-isolated compounds were recorded in the 400–4000 cm^{-1} range and with 0.5 cm^{-1} spectral resolution, using a Nicolet 6700 Fourier transform infrared (FTIR) spectrometer, equipped with a deuterated triglycine sulfate (DTGS) detector and a Ge/KBr beam splitter. The optical bench was continuously purged with a flux of dry and CO_2 filtered N_2, to avoid interference from atmospheric H_2O and CO_2.

Matrix isolation EPR spectroscopy measurements

A 100 mM solution of compound 1 in MeTHF (100 μL) was degassed under high vacuum ($\sim 3.0 \times 10^{-2}$ Pa) in a quartz EPR tube, which was sealed after three freeze-pump-thaw cycles under the vacuum conditions. The MeTHF solution of compound 1 was irradiated in the EPR cavity at 10 K. The X-band EPR signals were obtained at a resonance frequency of 9.40 GHz using a Bruker E500 spectrometer at 10-50 K.

In situ UV irradiation experiments

In the steady state infrared spectroscopy experiments carried out in Ar and N_2 matrices, *in situ* UV irradiation of the samples was undertaken using different approaches. In the case of the experiments carried out in the Ar matrices, broadband UV radiation was used, as provided by the KBr external window of the cryostat and water filtered (≥ 290 nm) light generated by a 500 W Hg(Xe) lamp (Newport, Oriel Instruments), with output power set to 200 W. For the experiments carried out in the N_2 matrices, tunable narrowband light was used (~0.1 cm^{-1} bandwidth; $\lambda = 290$ nm; pulse energy ~8 mJ), provided by a Spectra Physics

Quanta-Ray MOPO-SL optical parametric oscillator (OPO) pumped with a pulsed Nd:YAG laser (repetition rate = 10 Hz, duration = 10 ns).

For the EPR measurements, the photolysis was conducted at 266 nm (5 mJ), using a Nd-YAG laser (Spectra Physics Indi-40).

Computational Details

Quantum chemistry computations were performed at both the B3LYP/6-311++G(3df,3dp) and M06-2X/6-311++G(3df,3dp) levels of theory[36-43], using Gaussian 09 (Revision D.01)[44]. Geometry optimizations were performed using the "tight" optimization criteria.

The harmonic vibrational wavenumbers and IR intensities were calculated at the same levels of theory and scaled in order to correct them for the neglect of anharmonicity, basis sets restraints and the effect of incomplete treatment of the electron correlation. The scaling factors were acquired by fitting the computed harmonic to the experimental IR wavenumbers of compound 1 within the 1900-600 cm^{-1} region and those of compounds **4** and **5** within the 1900-500 cm^{-1} (see Figure S1 in the Supporting Information). The slopes obtained by least-squares linear fit, intercepting zero ($y = bx$), were then used to scale the computed harmonic wavenumbers of the photoproducts and reactant in the 1900-400 cm^{-1} range. The simulation of the IR spectra was achieved using the calculated (scaled) wavenumbers and IR intensities (in km mol^{-1}), which were convoluted with Lorentzian functions with a full-width at half-maximum (fwhm) of 2 cm^{-1}.

RESULTS AND DISCUSSION

Photoinduced reactivity of* 1 *in low temperature solid Ar and N_2 matrices

B3LYP and M06-2X density functional theory calculations, with the 6-311++G(3df,3pd) basis set, were performed on the studied dispiro-1,2,4-trioxolane (adamantane-2-spiro-3'-8'-oxo-1',2',4'-trioxaspiro[4,5]decane; **1**). Both methods predict the existence of two conformers of the compound with similar energies (see Table 1), which are represented in Figure 1. The two conformers differ in the orientation of the spiro-*p*-cyclohenanonyl moiety, which in the most stable form (A) is turned to the peroxide group and in the less stable one (B) is oriented towards the ring ether fragment. Their population ratio (A:B) in the room

temperature (298.15 K) gas phase equilibrium is expected to stay between 1.1 and 1.5 (which are the values resulting from the relative energies obtained in the B3LYP and M06-2X calculations, respectively), *i.e.*, both forms are predicted to be significantly populated in these experimental conditions, and can then be expected to be present in the cryogenic matrices investigated in this work (see below). The Cartesian coordinates of the two conformers, as predicted by the two methods used in this study, are provided as Supporting Information (Tables S1 and S2).

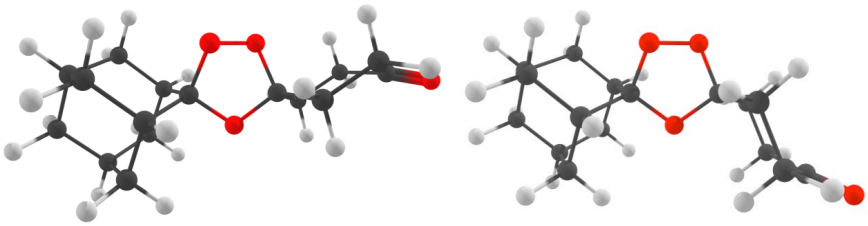

Figure 1. B3LYP/6-311++G(3df,3pd) optimized structures of the two conformers of **1** in the electronic ground state (S_0).

Table 1. B3LYP/6-311++G(3df,3pd) and M06-2X/6-311++G(3df,3pd) calculated energies (kJ mol^{-1}) for the conformers of **1** (see Figure 1) zero-point energies (ZPE) and estimated room temperature (298.15 K) percent populations in the gas phase equilibrium.

	B3LYP		**M06-2X**	
	1A	**1B**	**1A**	**1B**
Energy	-2426219.58	-2426218.50	-2425270.01	-2425269.82
ZPE	954.83	954.74	966.62	966.59
Energy (with ZPE)	-2425264.75	-2425263.76	-2424303.39	-2424303.22
ΔEnergy	0.00	0.99	0.00	0.17
Population (298.15 K)	59.8 %	40.2 %	51.7 %	48.3 %

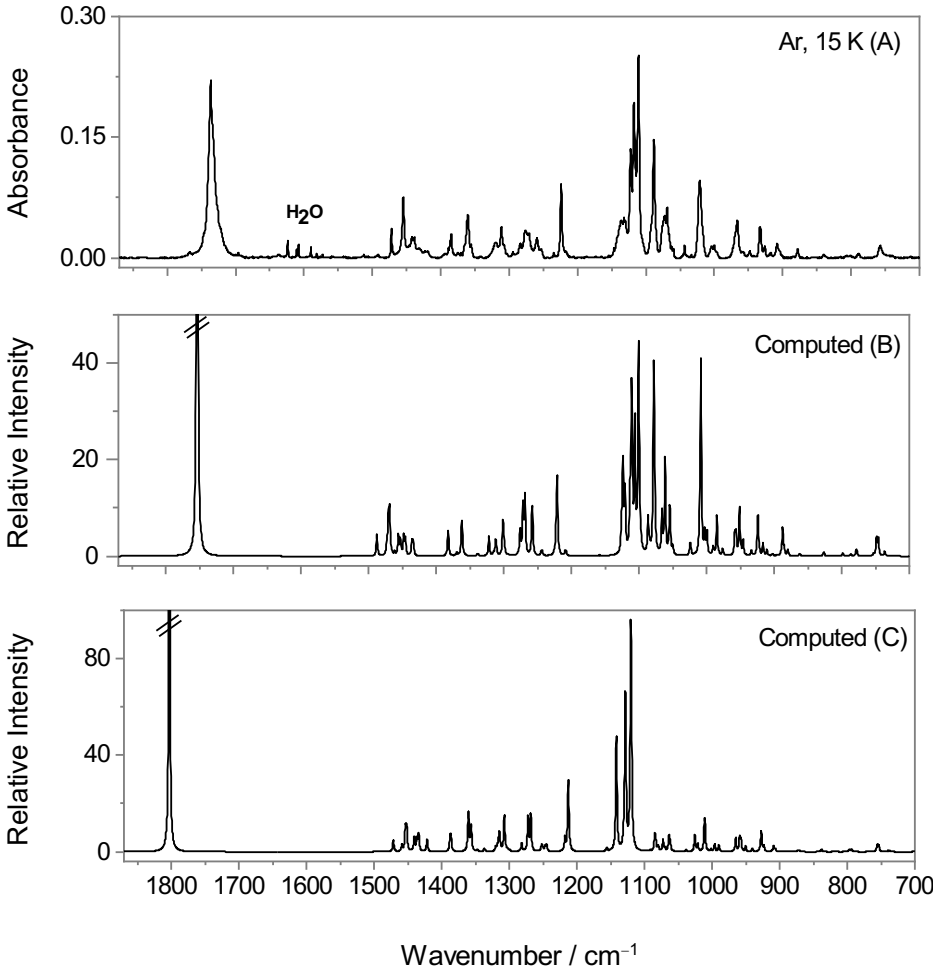

Figure 2. Infrared spectra of **1**: (A) isolated in an Ar matrix (15 K); (B), (C) calculated using the B3LYP and M06-2X functionals (with the 6-311+G(3df,3pd) basis set). The calculated spectra are shown as the 1:1 sum of the spectra of both conformers of the compound, and the frequencies were scaled by 0.983 and 0.971 factors in (B) and (C), respectively. The spectrum observed in the N_2 matrix is very similar to that obtained in argon and is provided in the Supporting Information (Figure S2).

The dispiro-1,2,4-trioxolane **1** was sublimed under high-vacuum at room temperature and co-deposited with large excess of argon or N_2 onto the cold (15 K) CsI substrate of the used cryostat. The infrared spectra of the prepared matrices were subsequently recorded. The spectrum obtained for the compound in the argon matrix is shown in Figure 2, while that obtained in the N_2 matrix is provided in the Supporting Information (Figure S2). The two spectra were found to be very similar, testifying the fact that the molecules of the compound were well-isolated in both matrices and also that the conformational population of **1** existing in the gas phase prior to deposition was efficiently trapped in the matrices. Also, the peroxide

1 was found not to undergo thermal decomposition upon sublimation under the used conditions for matrix deposition. The spectroscopic data (both experimental and calculated frequencies and intensities) are summarized in Tables S3-S5 (Supporting Information). It can be seen that, in spite of the similarity of the spectra of the two conformers, several bands observed in the experimental spectra could be assigned to the individual forms, thus confirming the presence of both conformers in the matrices.

The comparison of the spectrum obtained in the argon matrix with those theoretically predicted (see Figure 2), shows that the B3LYP functional reproduces better the experimental data throughout the spectrum than the M06-2X functional. Thus, spectra calculated using the B3LYP functional will be used in this study for the analysis of the experimentally obtained spectroscopic data of the remaining compounds under study.

The UV-induced reactivity of **1** was investigated in the two types of matrices used (Ar, N_2). Argon matrix was used as standard work medium, while N_2 matrix, known to stabilize high-energy species by establishing specific interactions with the guest species[45,46], was chosen to check the possibility of detection in this medium of any putative reaction intermediate. Both broadband ($\lambda \geq 290$ nm) and narrowband ($\lambda = 290$ nm) excitations were applied. The irradiations were performed at wavelengths within the observed band in the UV-vis spectra of **1** in ethanol solution (Figure S3). The results were found to be qualitatively identical in both matrices and for the two excitation procedures followed. Upon excitation, the bands initially present in the spectra reduced in intensity, while new bands started to emerge, indicating conversion of the trioxolane **1** into other chemical species. Particularly noticeable new spectral features were observed in the ν(C=O), (between 1720-1750 cm^{-1}) and ν(C-O), (1080-1120 cm^{-1}) regions. The intensities of the bands of **1** and those of the new bands changed continuously with the irradiation time, until almost complete conversion of the reactant **1** (after ~30 min. of broadband irradiation of the compound in an argon matrix). Detailed analysis of the spectra of the photolysed matrices allowed identification of the observed photolysis products as being 4-oxahomoadamantan-5-one **4** and 1,4-cyclohexanedione **5**, the expected final products for the photolysis of the trioxolane **1**, initiated by homolytic cleavage of the labile peroxide bond. This can be clearly seen in Figure 3, where the experimental difference IR spectrum (spectrum obtained after 30 min. of irradiation at $\lambda \geq 290$ nm *minus* spectrum of the as-deposited argon matrix) is compared with

the B3LYP/6-311++G(3df,3pd) calculated difference IR spectrum generated by subtracting the calculated spectrum of **1** from the sum of the spectra of **4** and **5** {in a ratio (0.5[4]+0.5[5]):1[1]}. The identification of the photoproducts was further confirmed by recording the IR spectra of genuine samples of **4** and **5** (see experimental section) deposited in argon matrices and *(i)* comparing these spectra with the spectra of the photoproducts generated upon UV irradiation of matrix isolated **1** (see Figure 4), or *(ii)* comparing the difference experimental IR spectrum shown in Figure 3 (irradiated *minus* as-deposited matrix spectra) with the one obtained by subtracting the experimental spectrum of **1** from the sum of the experimentally obtained IR spectra of the genuine samples of **4** and **5** isolated in argon matrices (see Figure 5).

The structural computed data obtained with the B3LYP and M06-2X functionals for **4** and **5** (graphical representation of the optimized minimum energy structures, and summary of calculated energy data), as well as the spectroscopic data obtained both theoretically and experimentally for these compounds (graphical comparison of the calculated and matrix isolation experimental infrared spectra of the compounds, and tables with calculated and experimental frequencies and intensities, those latter including the bands of **4** and **5** both in the photolysed matrices of **1** and as isolated species) are given in the Supporting Information (Tables S6-S14 and Figures S4 and S5). The B3LYP computed vibrational frequencies of **4** and **5** were scaled by 0.983 and 0.982, respectively.

According to the obtained results , the diradical rearrangement is regioselective , with no evidence of formation of the alternative products, 2-adamantanone and oxocane-2,7-dione. This can be clearly seen when one compares the infrared spectra of the photoproduced species, generated after UV irradiation of the matrix-isolated **1**, with those of 2-adamantanone and oxocane-2,7-dione (see Figure 3; additional calculated structural and spectroscopic data on these two compounds are presented in the Supporting Information, Figure S6 and Tables S15 and S16). The observed regioselectivity can be explained by the expected greater stability of the (secondary carbon-centered)/oxygen-centered diradical species **3**, in comparison with the putative alternative (primary carbon-centered)/oxygen-centered diradical that would lead to the non-observed final products. In addition, spin density calculations (performed at the B3LYP/6-311++G(3df,3dp) level) on the triplet state dioxygen-centered diradical result in a considerable larger electron spin density in the tertiary

β-carbon of the spiroadamantyl substituent as compared to that of the secondary β-carbon of the spiro-*p*-cyclohexanonyl substituent, which can also be considered an indication of a most favorable rearrangement of the initially generated dioxygen-centered diradical into the (secondary carbon-centered)/oxygen-centered diradical species **3**, leading to the observed final products.

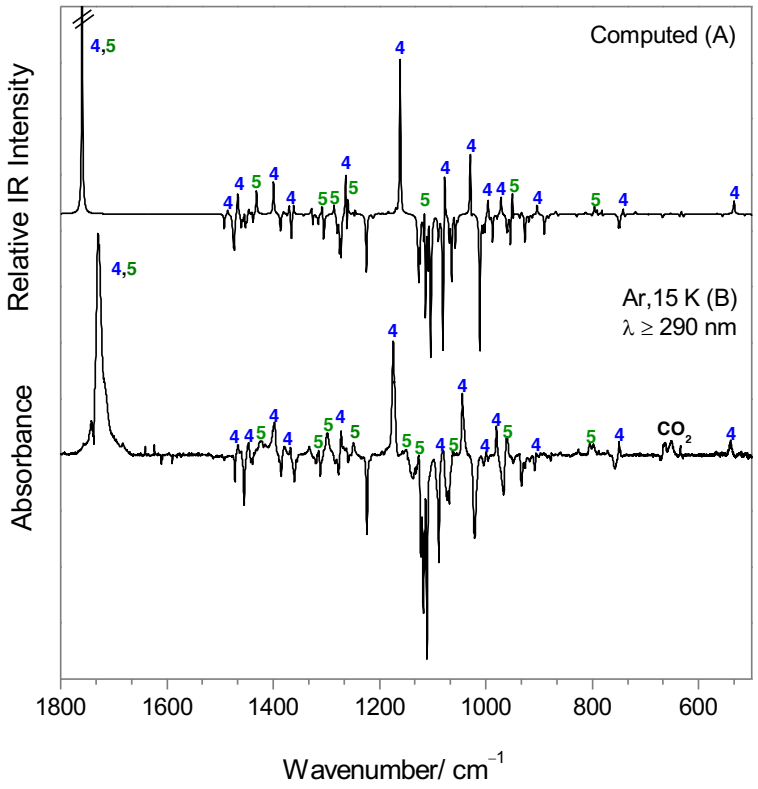

Figure 3. (A) B3LYP/6-311++G(3df,3pd) calculated difference IR spectrum: spectra of 4-oxahomoadamantan-5-one **4** and 1,4-cyclohexanedione **5** *minus* the spectrum of **1** [in a ratio (0.5+0.5):1]. (B) Experimental difference IR spectrum: spectrum after irradiation at λ ≥ 290 (30 min.; Ar matrix at 15 K) *minus* spectrum of the as-deposited matrix. The negative bands were assigned to **1**; the positive ones were assigned to the new photogenerated species **4** and **5**.

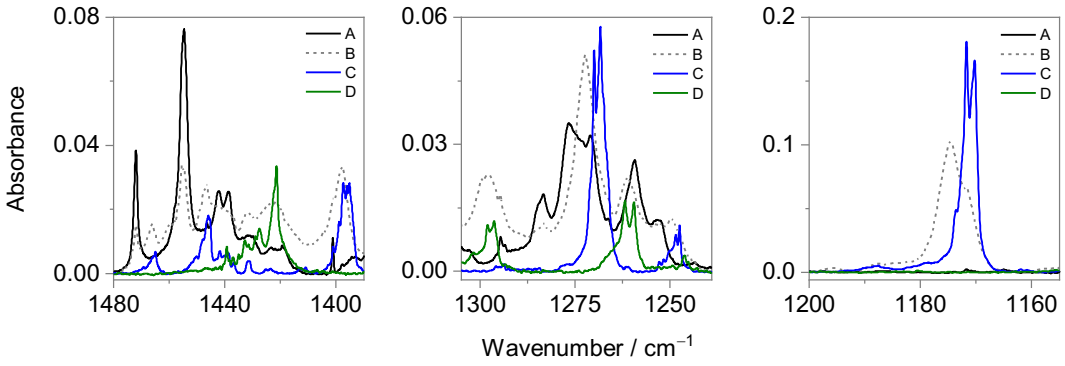

Figure 4. Comparison of selected regions of the experimental IR spectrum obtained before irradiation of the matrix isolated **1** (Ar matrix at 15 K) (solid black line; A) with the spectrum collected after 30 min of λ ≥ 290 irradiation (dashed gray line; B) and with the spectra of authentic samples of 4-oxahomoadamantan-5-one **4** (solid blue line; C) and 1,4-cyclohexanedione **5** (solid green line; D) isolated in argon at 15 K.

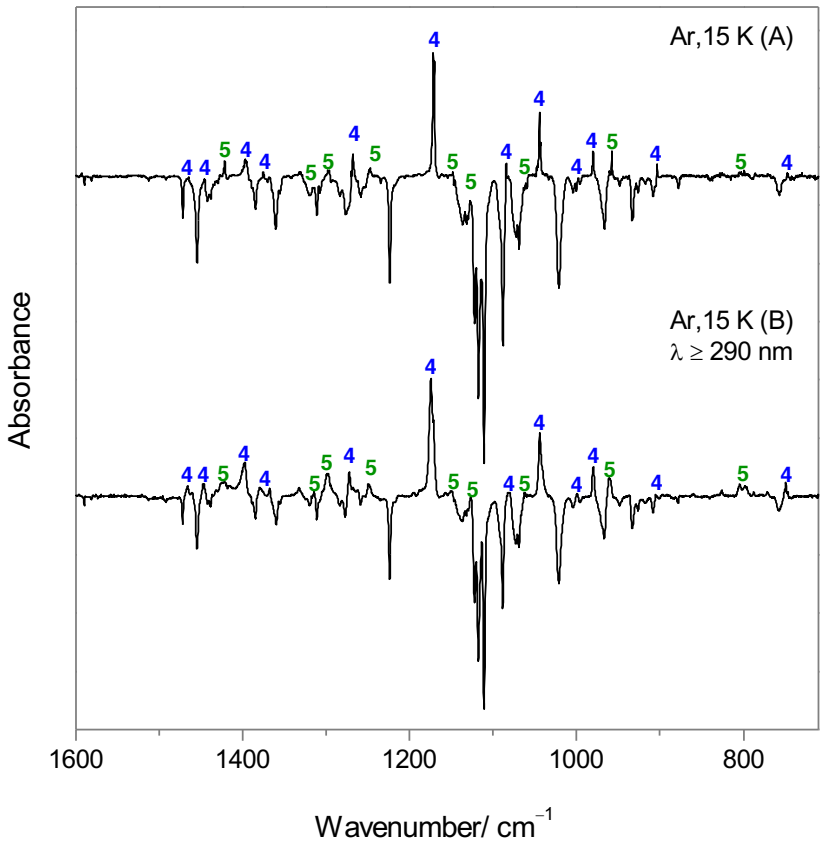

Figure 5. (A) Experimental difference IR spectrum: spectra of authentic samples of matrix isolated 4-oxohomoadamantan-5-one **4** and authentic 1,4-cyclohexanedione **5** *minus* spectrum of **1** ☐Ar

matrix at 15 K). (B) Experimental difference IR spectrum: spectrum after irradiation of matrix isolated **1** ($\lambda \geq 290$; 30 min) *minus* spectrum of the as-deposited matrix (Ar matrix at 15 K).

EPR detection of the dioxygen-centered 2 and carbon-centered/oxygen-centered 3 diradicals

The *in situ* EPR measurements in the photolysis of **1** in MeTHF matrix were conducted using 266 nm laser light (5 mJ) at 10-50 K. The X-band EPR signals were measured at a resonance frequency of 9.40 GHz (Figure 6). During the photolysis at 10 K (Figure 6 Ib), a half-field signal at ~1550 G (triplet species A) was observed after 120 seconds, which is a typical triplet species of diradicals, and another half-field signal at 1670 G (triplet species B) was detected after 420 seconds, together with the 1550 G signal (Figure 6 Ic). Both resonance frequencies (1550 and 1670 GHz) are typical for triplet diradicals. Under dark conditions, only the half-field signal at 1670 G was detected (Figure 6 Id), indicating that the disappeared triplet species A is short-lived, while the triplet species B is persistent, under the MeTHF matrix conditions, at 10 K.

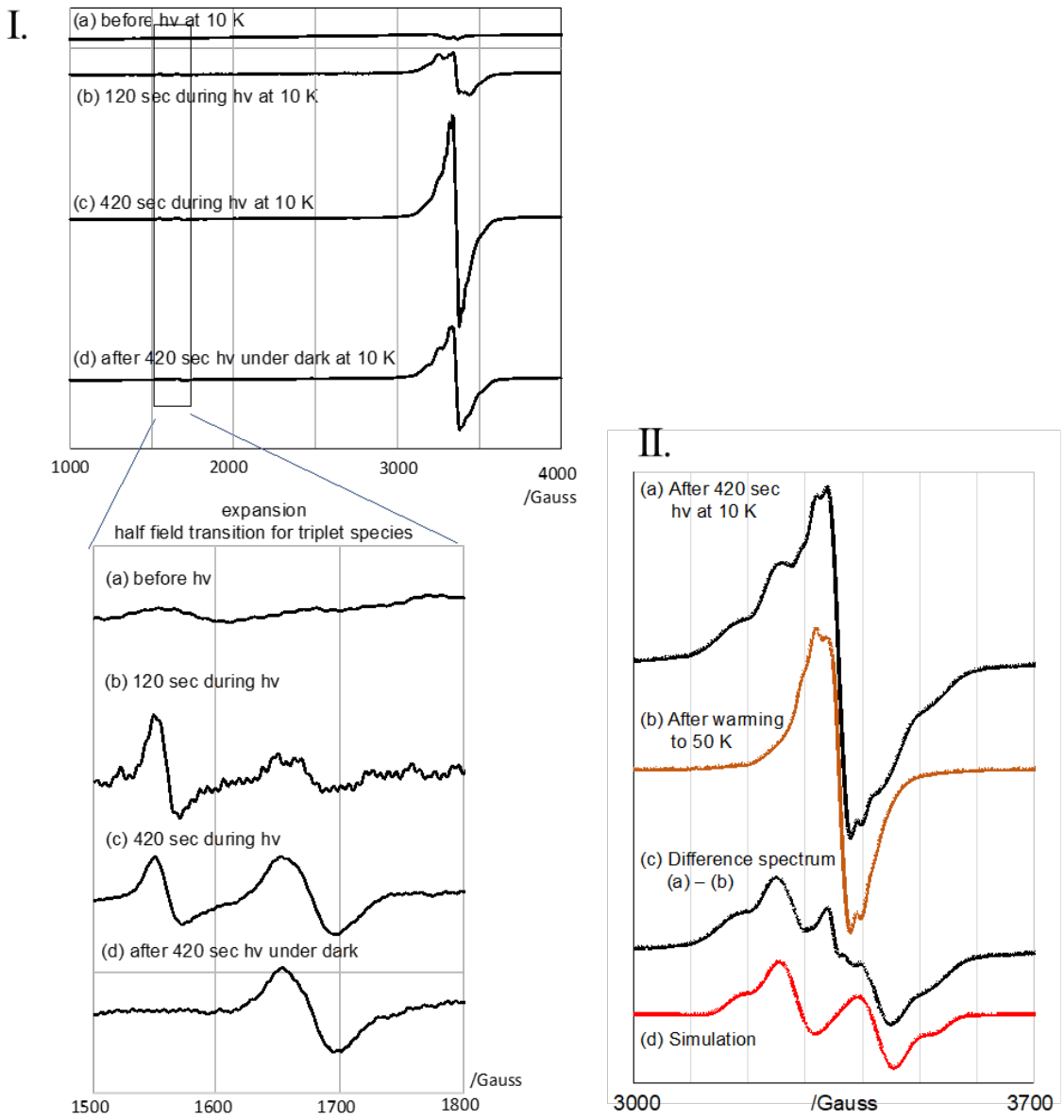

Figure 6. **I**: X-band EPR spectra (9.40 GHz, 1000-4000 G) obtained from photolysis studies of compound 1 (100 mM) in MeTHF-matrix, at 266 nm; (a) before irradiation at 10 K; (b) after irradiation for 120 seconds at 10 K; (c) after irradiation for 420 seconds, at 10 K; (d) after irradiation for 420 seconds, under dark, at 10 K; **II**: X-band EPR signals (9.40 GHz, 3000-4000 G) from photolysis of compound **1** (100 mM) in MeTHF-matrix at 266 nm; (a) after 420 seconds photolysis, under dark, at 10 K; (b) after warming the sample to 50 K, and subsequent re-cooling to 10K; (c) difference spectrum between (a)–(b); (d) simulated spectrum with $D/hc = 0.160$ cm^{-1} and $E/hc = 0.001$ cm^{-1} at g value of 2.003.

To gather further insight regarding the reactivity of the triplet species B, the photolystate at 10 K was warmed to 50 K under dark conditions (Figure 6 IIb). The typical triplet signal disappeared and did not recover to the original one in Figure 6 Ic after re-cooling the sample to 10 K, indicating that the triplet species B was also thermally labile at ~50 K. The triplet signal of B was obtained by the difference spectrum of Figure 6 IIa–b (Figure 6 IIc). The zero-field splitting parameters *D*/hc and *E*/hc of the triplet species B were determined to be 0.160 cm^{-1} and 0.001 cm^{-1} after the simulation (Figure 6 IId). From the *D*/hc value, the distance between two spins was estimated to be ~ 5 Å.

The EPR results demonstrate that two triplet species (A and B) are formed during the photolysis of the studied trioxolane **1**, in agreement with the expectations. One of the triplet species (A) is thermally quite labile, while the other (B) is persistent at 10 K. Considering the results obtained in the photolysis of **1** in argon matrix, in particular the obtained final products, the theoretical data described in the previous sections, and the accumulated literature evidence, diradicals **2** and **3** shall be assigned to the intermediates A and B, respectively, detected by EPR. This is the first experimental detection of these diradical intermediates.

CONCLUSIONS

Adamantane-2-spiro-3'-8'-oxo-1',2',4'-trioxaspiro[4,5]decane **1**, a reported potent antiparasitic dispiro-1,2,4-trioxolane, has been synthesized and studied from the view point of its molecular structure and monomeric photochemistry, using matrix isolation techniques coupled to FTIR and EPR spectroscopy. It is noteworthy that the ozonide **1** remained thermally stable upon sublimation required for matrix deposition. All experimental results have been supported by quantum chemical calculations using two levels of theory [B3LYP/6-311++G(3df,3dp) and M06-2X/6-311++G(3df,3dp)], the comparison of the spectrum obtained in the argon matrix with those theoretically predicted showing that the B3LYP functional reproduces better the experimental data throughout the spectrum than the M06-2X functional. Both methods predict two conformers for the dispiro-1,2,4-trioxolane **1** with very close energies, differing in the orientation of the spiro-*p*-cyclohenanonyl moiety, which in the most stable form is directed to the peroxide group, while in the less stable one is oriented towards the ring ether fragment. In the experimental spectra, several bands were

observed which permitted the assignment of the individual forms, thus confirming the presence of both conformers in the matrices.

The UV-induced reactivity of **1** was investigated in the two types of matrices (Ar, N_2), using broadband ($\lambda \geq 290$ nm) and narrowband ($\lambda = 290$ nm) irradiation, the results proving qualitatively identical in both matrices and for the two followed excitation procedures. Irradiation of matrix-isolated **1** at $\lambda \geq 290$ nm resulted in photocleavage of the trioxolane pharmacophore with formation of other chemical species, as evidenced by the observation of new spectral features in the ν(C=O), (between 1720-1750 cm^{-1}) and ν(C-O), (1080-1120 cm^{-1}) regions. Detailed analysis of the spectra of the photolyzed matrices allowed identification of 4-oxahomoadamantan-5-one **4** and **1**,4-cyclohexanedione **5** as the sole final products from photolysis of the trioxolane **1**. This identification was further confirmed through comparison with the matrix spectra of the pure compounds. Such observation indicates that the dioxygen-centered diradical **2**, formed upon homolytic cleavage of the labile peroxide bond, undergoes a regioselective radical isomerization to form the more stable (secondary carbon-centered)/oxygen-centered diradical **3**. In fact, no evidence was observed for the formation of 2-adamantanone and oxocane-2,7-dione, the products that would arise from the putative alternative (primary carbon-centered)/oxygen-centered diradical. The observed regioselectivity can be explained by the expected greater stability of the (secondary carbon-centered)/oxygen-centered diradical species **3** in comparison to its primary counterpart. Spin density calculations (performed at the B3LYP/6-311++G(3df,3dp) level) on the triplet state dioxygen-centered diradical result in a considerably larger electron spin density in the tertiary β-carbon of the spiroadamantyl substituent as compared to that of the secondary β-carbon of the spiro-*p*-cyclohexanonyl substituent, which can also be taken as an indication of a most favorable rearrangement of the initially generated dioxygen-centered diradical into the (secondary carbon-centered)/oxygen-centered diradical species **3**, leading to the final products identified. These results are in keeping with information gathered from studies on the mechanisms of bioactivation and action of trioxolane based antiparasitic candidates, where heme-adducts of the secondary carbon-centered)/oxygen-centered diradical species analogues of **3** were detected[47].

In situ EPR measurements during photolysis of compound **1** deposited in a MeTHF-matrix led to the detection of signals at1550 and 1670 GHz, corresponding to resonances of

two triplet diradicals, the one at 1550 GHz appearing thermally labile while the other (1670 GHz) proved persistent at 10 K. The observation of signals with resonance frequencies that are typical for triplet diradicals, combined with the product characterizations achieved through the matrix isolation FTIR studies, indicate that the postulated diradicals **2** and **3** shall correspond to the intermediates detected by the experiment.

In conclusion, our results support the proposal of a regioselective radical isomerization of dioxygen-centered diradical **2** to afford the (secondary carbon-centered)/oxygen-centered diradical **3**, also providing evidence for the presence of both intermediate diradicals on a photolyzed MeTHF-matrix containing compound **1**. This work deepens the knowledge concerning the photoreactivity/photostability of antiparasitic endoperoxides based on the trioxolane pharmacophore.

ASSOCIATED CONTENT

Supporting Information. Supplemental figures and calculated data for adamantane-2-spiro-3'-8'-oxo-1',2',4'-trioxaspiro[4,5]decane. This material is available free of charge via the Internet at http://pubs.acs.org

AUTHOR INFORMATION

Corresponding Author

* E-mail: rfausto@ci.uc.pt

* E-mail: mcristi@ualg.pt

Notes

The authors declare no competing financial interest.

Author Contributions

The authors contributed equally.

ACKNOWLEDGEMENTS

The Coimbra Chemistry Centre (CQC) and the Center of Marine Sciences (CCMar) are supported by the Portuguese Science Foundation (FCT; Projects UID/QUI/0313/2019 and

UID/MULTI/04326/2019) and COMPETE-EU. E.M.B. thanks FCT for both the Research Grants CCMAR/BI/0013/2017, awarded within the Project PTDC/MAR-BIO/4132/2014, and SFRH/BD/136246/2018. L.I.L.C. thanks FCT and CCMar for the Research Grant CCMAR/BI/0017/2016 awarded within the Project PTDC/MAR-BIO/4132/2014. P.S.M.A. thanks FCT for the Research Grant SFRH/BD/130407/2017.

REFERENCES

1. Tu, Y. Y. The discovery of artemisinin (qinghaosu) and gifts from Chinese medicine, *Nature Med*., **2011**, *17*, 1217–1220.
2. Tu, Y. Y. Artemisinin - A Gift from Traditional Chinese Medicine to the World (Nobel Lecture). *Angew. Chem. Int. Ed*., **2016**, *55*, 10210–10226.
3. Liu, C. X. Discovery and Development of Artemisinin and Related Compounds. *Chin. Herb. Med*., **2017**, *9*, 101–114.
4. Jefford C. W. Why Artemisinin and Certain Synthetic Peroxides are Potent Antimalarials. Implications for the Mode of Action. *Curr. Med. Chem*., **2011**, *8*, 1803–1826.
5. Cumming, J. N.; Polypradith, P.; Posner, G. H. Antimalarial Activity of Artemisinin (Qinghaosu) and Related Trioxanes: Mechanism(s) of Action. *Adv. Pharmacol*., **1996**, *37*, 253–297.
6. Wu, Y. How Might Qinghaosu (Artemisinin) and Related Compounds Kill the Intraerythrocytic Malaria Parasite? A Chemist's View. *Acc. Chem. Res*., **2002**, *35*, 255–259.
7. Robert, A.; Coppel, Y.; Meunier, B. Alkylation of heme by the antimalarial drug artemisinin. *Chem. Commun*., **2002**, 414–415.
8. Meshnick, S. R.; Artemisinin: mechanisms of action, resistance and toxicity. *Int. J. Parasitol*., **2002**, *32*, 1655–1660.
9. Eckstein-Ludwig, U.; Krieger, J.; Smeilus, T.; Kaiser, M.; Seo, E. J.; Efferth, T.; Ginannis, A. Total Synthesis and Biological Investigation of (-)-Artemisinin: The Antimalarial Activity of Artemisinin Is not Stereospecific. *Angew. Chem. Int. Ed*., **2018**, *57*, 8293–8296.

10. Tilley, L.; Straimer, J.; Gnädig, N. F.; Ralph, S. A.; Fidock, D. A. Artemisinin Action and Resistance in *Plasmodium falciparum*. *Trends Parasit*., **2016**, *32*, 682–696.
11. Winzeler, E. A.; Manary, M. J. Drug resistance genomics of the antimalarial drug artemisinin. *Gen*. *Biol*., **2014**, *15*, 544.
12. Cravo, P.; Napolitano, H.; Culleton, R. How genomics is contributing to the fight against artemisinin-resistant malaria parasites. *Acta Tropica*, **2015**, *148*, 1–7.
13. Wang, J.; Zhang, C.; Chia, W.; Loh, C.; Li, Z.; Lee, Y.; He, Y.; Yuan, L.; Lim, T.; Liu, M. et al. Haem-activated promiscuous targeting of artemisinin in *Plasmodium falciparum*. *Nature Comm*., **2015**, *6*, Art. Nº 10111 (1–11).
14. Aweeka, F. T.; German, P. I. Clinical Pharmacology of Artemisinin-Based Combination Therapies. *Clin*. *Pharmacokin*., **2008**, *47*, 91–102.
15. Sugimone, H. H. In *Handbook of Organic Photochemistry and Photobiology*. Horspool, W. M.; Song, P. S. Eds.; CRC Press, London, **1994**, pp 1229–1253 references therein.
16. Jefford, C. W.; Rossier, J. C.; Boukouvalas, J. Eliminative ring fission of 1,2,4-trioxan-5-ones. A new approach to α-keto acids. *J*. *Chem*. *Soc*. *Chem*. *Commun*., **1986**, 1701–1702.
17. Jefford, C. W.; Rossier, J. C.; Boukouvalas, J. A Mild and Efficient Preparation of cis-1,2-Diols from 1,2,4-Trioxanes. *J*. *Chem*. *Soc*. *Chem*. *Commun*., **1987**, 1593–1594.
18. Jefford, C. W.; Kohmoto, S.; Rossier, J. C.; Boukouvalas, J. Chemistry of 1,2,4-Trioxanes. Formation of 1,2-Diol Monoesters. *J*. *Chem*. *Soc*. *Chem*. *Commun*., **1985**, 1783–1784.
19. Jefford, C. W.; Rossier, J. C.; Boukouvalas, J. 1,2,4-Trioxanes as masked, dual purpose, functional groups. *Heterocycles*, **1989**, *28*, 673–676.
20. Jefford, C. W.; Rossier, J. C.; Boukouvalas, J. Electrophile-induced rearrangement of 1,2,4-trioxanes. Formation of 1-benzofuran and 2H-1-benzopyrans. *J*. *Chem*. *Soc*. *Chem*. *Commun*., **1987**, 713–714.
21. Erhardt, S.; Macgregor, S. A.; McCullough, K. J.; Savill, K.; Taylor, B. J. Model Studies of β-Scission Ring-Opening Reactions of Cyclohexyloxy Radicals:

510 Application to Thermal Rearrangements of Dispiro-1,2,4-trioxanes. *Org. Lett.*, **2007**,
511 *9*, 5569–5572.
512 22. Tang, Y.; Dong, Y.; Wang, X.; Sriraghavan, K.; Wood, J. K.; Vennerstrom J. L.
513 Dispiro-1,2,4-trioxane Analogues of a Prototype Dispiro-1,2,4-trioxolane:
514 Mechanistic Comparators for Artemisinin in the Context of Reaction Pathways with
515 Iron(II). *J. Org. Chem.*, **2005**, *70*, 5103–5110.
516 23. Haq, A.; Kerr, B.; McCullough K. J. A Rapid Route to Medium to Large Ring
517 Lactones via the Thermolysis of Dispiro-1,2,4-trioxane Derivatives. *J. Chem. Soc.*
518 *Chem. Commun.*, **1993**, 1076–1078.
519 24. Abe, M.; Adam, W.; Heidenfelder, T.; Nau, W. M.; Zhang, X.; Intramolecular and
520 Intermolecular Reactivity of Localized Singlet Diradicals: The Exceedingly Long-
521 Lived 2,2-Diethoxy-1,3-diphenylcyclopentane-1,3-diyl. *J. Am. Chem. Soc.*, **2000**,
522 *122*, 2019–2026.
523 25. Abe, M.; Inakazu, T.; Munakata, J.; Nojima, M. ^{18}O-Tracer Studies of Fe(II)-Induced
524 Decomposition of 1,2,4-Trioxolanes (Ozonides) Derived from Cyclopentenes and
525 Indenes. Inner-Sphere Electron Transfer Reduction of the Peroxide Linkage. *J. Am.*
526 *Chem. Soc.*, **1999**, *121*, 6556–6562.
527 26. Meyer, B. *Low Temperature Spectroscopy*, American Elsevier Publishers Company;
528 New York (USA), **1971**.
529 27. Andrews L.; Moskovits, M. *Chemistry and Physics of Matrix Isolated Species*. Eds.,
530 Elsevier, Amsterdam (Holland), **1989**.
531 28. Barnes, A.; Orville-Thomas, W. J.; Gaufrhs, R.; Muller, A. *Matrix Isolation*
532 *Spectroscopy*. Eds.; Springer; Dordrecht (Holland), **1981**.
533 29. Dunkin, I. R. *Matrix Isolation Techniques: A Practical Approach*. Oxford University
534 Press; Oxford (UK), **1998**.
535 30. Fausto, R. *Low Temperature Molecular Spectroscopy*. Ed., NATO-ASI Series C483;
536 Kluwer, Amsterdam (Holland), **1996**.
537 31. Vennerstrom, J. L.; Dong, Y.; Chollet, J.; Matile, H. Spiro and dispiro 1,2,4-
538 trioxolane antimalarials. U.S. patent. 6,486,199B1, **2002**.
539 32. Lobo, L.; Cabral, L. I. L.; Sena, M. I.; Guerreiro, B. Rodrigues, A. S.; Andrade-Neto,
540 V. F.; Cristiano, M. L. S.; Nogueira, F. New endoperoxides highly active *in vivo* and

in vitro against artemisinin-resistant *Plasmodium falciparum*. *Malar. J.*, **2018**, *17*, 1–11.

33. Cortes, S.; Albuquerque, A.; Cabral, L. I. L.; Lopes, L.; Campino, L.; Cristiano, M. L. S. *In vitro* susceptibility of *Leishmania infantum* to Artemisinin derivatives and selected trioxolanes. *Antimicrob. Agents Chemother*. **2015**, *59*, 5032–5035.
34. Araujo, N.C.P.; Afonso, R.; Beringela, A.; Cancela, M.L.; Cristiano, M.L.S.; Leite, R.B. Peroxides with antiplasmodial activity inhibit proliferation of *Perkinsus olseni*, the causative agent of Perkinsosis in bivalves. *Parasitol. Int.*, **2013**, *62*, 575–582.
35. Renoud-Grappin, M.; Vanucci, C.; Lhommet, G. Diastereoselective synthesis of a limonoid model related to the insect antifeedant genudin. *J. Org. Chem.*, **1994**, *59*, 3902–3905.
36. Raghavachari, K.; Binkley, J. S.; Seeger, R.; Pople, J. A. Selfconsistent molecular orbital methods. XX. A basis set for correlated wave functions. *J. Chem. Phys.*, **1980**, *72*, 650–654.
37. Frisch, M. J.; Pople, J. A.; Binkley, J. S. Selfconsistent molecular orbital methods 25. Supplementary functions for Gaussian basis sets, *J. Chem. Phys.*, **1984**, *80*, 3265–69.
38. Becke, A. D. Density-functional thermochemistry. III. The role of exact exchange. *J. Chem. Phys.*, **1993**, *98*, 5648–5652.
39. Lee, C.; Yang, W.; Parr, R. G. Development of the Colic-Salvetti correlation-energy formula into a functional of the electron density. *Phys. Rev. B*, **1988**, *37*, 785–789.
40. Vosko, S. H.; Wilk, L.; Nusair, M. Accurate spin-dependent electron liquid correlation energies for local spin density calculations: a critical analysis. *Can. J. Phys.*, **1980**, *58*, 1200–1211.
41. Stephens, P. J.; Devlin, F. J.; Chabalowski, C. F.; Frisch, M. J. F. *Ab Initio* Calculation of Vibrational Absorption and Circular Dichroism Spectra Using Density Functional Force Fields. *J. Phys. Chem.*, **1994**, *98*, 11623–11627.
42. Zhao, Y.; Truhlar, D. G. The M06 suite of density functionals for main group thermochemistry, thermochemical kinetics, noncovalent interactions, excited states, and transition elements: two new functionals and systematic testing of four M06-class functionals and 12 other functionals. *Theor. Chem. Acc.*, **2008**, *120*, 215–241.

571 43. Zhao, Y.; Truhlar, D. G. Density Functionals with Broad Applicability in Chemistry.
572 *Acc. Chem. Res.*, **2008**, *41*, 157–167.
573 44. Frisch, M. J.; Trucks, G. W.; Schlegel, H. B.; Scuseria, G. E.; Robb, M. A.;
574 Cheeseman, J. R.; Scalmani, G.; Barone, V.; Mennucci, B.; Petersson, G. A. et al.
575 Gaussian 09, Revision D.01; Gaussian, Inc.; Wallingford, CT, **2004**.
576 45. Lopes, S.; Domanskaya, A. V.; Fausto, R.; Räsänen, M.; Khriachtchev, L. Formic
577 and acetic acids in a nitrogen matrix: Enhanced stability of the higher-energy
578 conformer. *J. Chem. Phys.*, **2010**, *133*, 144507.
579 46. Kus, N.; Fausto R. Effects of the matrix and intramolecular interactions on the
580 stability of the higherenergy conformers of 2-fluorobenzoic acid. *J. Chem. Phys.*,
581 **2017**, *146*, 124305.
582 47. Gibbons, P.; Verissimo, E.; Araujo, N. C.; Barton, V.; Nixon, G. L.; Amewu, R. K.;
583 Chadwick, J.; Stocks, P. A.; Biagini, G. A. B.; Srivastava, A. et al. Endoperoxide
584 Carbonyl Falcipain 2/3 Inhibitor Hybrids: Toward Combination Chemotherapy of
585 Malaria through a Single Chemical Entity. *J. Med. Chem.*, **2010**, *53*, 8202-8206.
586
587